Available online at www.sciencedirect.com
ScienceDirect
Cement and Concrete Research 37 (2007) 96–106
Cement and Concrete Research

Resistance of concrete protected by fabric to projectile impact

Fariborz Vossoughi [a], Claudia P. Ostertag [a,*], Paulo J.M. Monteiro [a], George C. Johnson [b]

[a] Department of Civil and Environmental Engineering, University of California, Berkeley, CA 94720, USA
[b] Department of Mechanical Engineering, University of California, Berkeley, CA 94720, USA

Received 29 April 2006; accepted 14 September 2006

Abstract

This paper reports on impact behavior of concrete panels protected by Polypropylene and Zylon fabric, respectively. Concrete panels were cast with different thickness and subjected to impact by a steel projectile. The initial and residual velocities were measured experimentally and the energy absorbed by the different concrete panels with and without fabric was calculated. All concrete panels were able to absorb almost all the kinetic energy of the projectiles. For concrete panels protected by fabric scabbing of concrete from the back face was considerably reduced and the debris contained by the fabric. Upper and lower bounds are proposed for energy absorbed per unit thickness and penetration results are compared with the available empirical formulas. It is shown that current penetration equations do not accurately predict impact parameters for concrete protected by fabric.

Keywords: Concrete; Impact; Projectile; Fabric; Penetration; Perforation; Energy

1. Introduction

Concrete structures may be required to withstand impact loads which can result, for example, from kinetic energy weapons, turbine blade fragments, and tornado generated projectiles. Impacting missiles are divided into "hard" or "soft" depending on the relative stiffness of the missile compared to the target. Missile impact can cause local and global damage to the structure [1–4]. Local damage can lead to concrete fragmentation from the front surface, projectile penetration into the target, scabbing of concrete from the back face, and finally, perforation through the target. The extent of damage depends on a variety of factors, such as impact velocity, mass, geometry, material properties of the projectile, and the material properties and thickness of the target [5]. Global damage consists of flexural deformation or macroscopic cracking which depends on the strain energy capacity of the target. To measure local damage, different indices have been proposed (Fig. 1), such as penetration depth (x), perforation thickness (h_e), scabbing thickness (h_s), and ballistic limit (v_{50}).

Currently, the local effects of the impact caused by the "hard" missile may be estimated using various empirical formulas based on data fitting of laboratory and in-situ test results [2,3]. However, these methods yield dimensionally inhomogeneous formulas, and are valid only for a short range of velocities. Moreover, they are based on tests performed on very thick elements. These problems are addressed using analytical and semi-empirical studies [6–8]. In the analytical methods, the governing equations are obtained by assuming one mode of failure. The two-stage model and the cavity expansion model are two popular analytical models. A combination of these two models has been also proposed recently [6]. In the two-stage model, the first stage is the dynamic penetration in which a bell-shaped plug is formed. During the second stage, the projectile pushes the plug and shears it off [3]. In the spherical cavity expansion model, the penetration of projectile is represented by the expansion of a spherical cavity at velocity v_c. Then, a closed-form solution between velocity of the projectile and the force exerted on it is obtained. Using this solution, the depth of penetration is obtained using Newton's second law [8–10]. Semi-empirical models, based on some theoretical basis, are also commonly used [11]. In all methods, dimensional analysis can be applied to make the impact parameters dimensionless so scaling of the results can be achieved more easily [12].

* Corresponding author.
E-mail address: ostertag@ce.berkeley.edu (C.P. Ostertag).

0008-8846/$ - see front matter © 2006 Elsevier Ltd. All rights reserved.
doi:10.1016/j.cemconres.2006.09.003

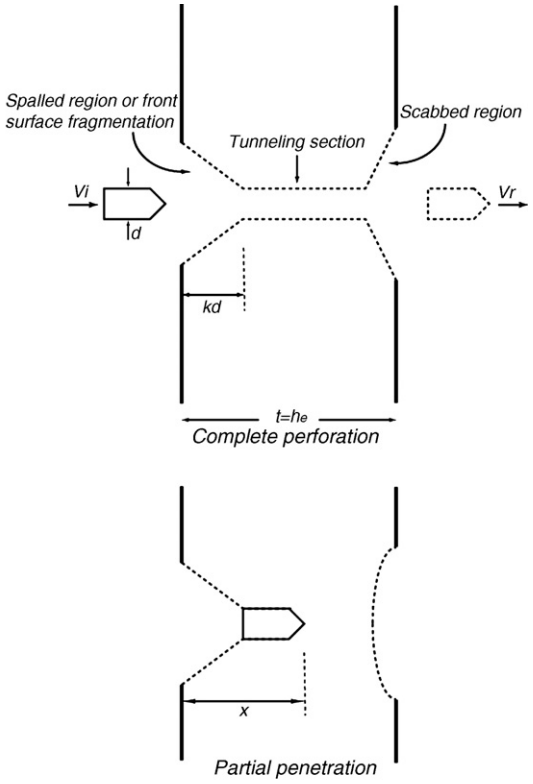

Fig. 1. Schematic view of complete perforation and partial penetration; kd=depth of conical entry crater; d=diameter of the projectile, h_e=perforation thickness, v_i=initial velocity of projectile, v_r=residual velocity of the projectile after perforation.

To protect concrete structures against impact, different methods can be employed [13]. One approach is to improve the concrete properties by increasing its strength or applying additional internal reinforcement, e.g., fiber-reinforced concrete. Varying results have been obtained for the strength approach. Test results on the resistance of high strength concrete (HSC) to projectile impact show that the penetration depth and crater diameter are reduced with an increase in the compressive strength [5]. However, in another study [14,15] HSC exhibits a larger crater surface area and hence a lower fracture energy under impact loading. Steel fibers are shown to be able to reduce the crater diameter and crack propagation, but their effect on penetration depth is not significant [16].

Another approach is to reduce damage by protecting the concrete with external elements [13]. These elements can act as a sacrificial layer. In this study, two types of fabric (Polypropylene, and Zylon) are used to protect or reinforce concrete externally. With this approach existing concrete structures can also be retrofitted.

2. Review of empirical and semi-empirical models

Available empirical models provide expressions for maximum penetration depth of a projectile that is impinging on a "thick target" in the normal direction. Based on the penetration depth into an infinitely thick sample, perforation and scabbing thicknesses are obtained. Perforation and scabbing thickness are the minimum thickness of the target to prevent perforation or scabbing, respectively. Numerous reviews of common methods have been published by different authors (Table 1) [6,17]. In this section only the modified National Defense Research Committee (NDRC) method and the cavity expansion model, which are commonly used, are presented in greater detail.

2.1. NDRC method

According to this method the impact force per unit contact area at any time is a function of both penetration depth and the instantaneous velocity. After some data fitting [2], and using Newton's second law, the penetration depth, x, is determined from:

$$\frac{x}{d}=\begin{cases}2\sqrt{G} & G\le 1.0 \text{ or } \frac{x}{d}\le 2\\ 1+G & G>1.0 \text{ or } \frac{x}{d}>2\end{cases}$$

$$G=\frac{3.8\times 10^{-5}NMV^{1.8}}{f_c'^{0.5}d^{2.8}} \tag{1}$$

Here, M is the projectile mass, d its diameter, V the initial velocity, f_c' the compressive strength of concrete, N the projectile nose shape factor (flat: 0.72; spherical: 1.00; and sharp: 1.14) and G a non-dimensional parameter. Since these formulas are not dimensionless, use of consistent units is important. Here, all the parameters are in SI units. Using regression analysis, the perforation and scabbing thicknesses are found from the following equations [2]:

$$\frac{h_s}{d}=\begin{cases}7.91\left(\frac{x}{d}\right)-5.06\left(\frac{x}{d}\right)^2 & \frac{x}{d}\le 0.65\\ 2.12+1.36\left(\frac{x}{d}\right) & 0.65<\frac{x}{d}\le 11.75\end{cases}$$

h_s : scabbing thickness (2)

$$\frac{h_e}{d}=\begin{cases}3.19\left(\frac{x}{d}\right)-0.718\left(\frac{x}{d}\right)^2 & \frac{x}{d}\le 1.35\\ 1.32+1.24\left(\frac{x}{d}\right) & 1.35<\frac{x}{d}\le 13.5\end{cases}$$

h_e : perforation thickness

The results of our experimental program are compared with the NDRC prediction and other empirical and semi-empirical models.

2.2. Cavity expansion models

Post-test concrete targets have a conical entry crater as shown in Fig. 1 with depth kd followed by a tunnel with the size of projectile diameter d. A value of k=2.0 has been suggested [6]. Therefore two regions are introduced in Eq. (1), $x/d\le 2$ for

Table 1
Empirical perforation formulas in SI units [6]

Formula	Penetration depth	Perforation thickness
Modified Petry	$\frac{x}{d}=3.39\times10^{-4}\frac{M}{d^3}\log_{10}\left(1+\frac{V^2}{19,974}\right)$	$\frac{h_e}{d}=2\frac{x}{d}$
ACE	$\frac{x}{d}=\frac{3.5\times10^{-4}}{\sqrt{f_c'}}\left(\frac{M}{d^3}\right)d^{0.215}V^{1.5}+0.5$ $I=\frac{MNV^2}{d^3f_c'}$	$\frac{h_e}{d}=1.23+1.07\frac{x}{d}$
Haldar formula	$\frac{x}{d}=-0.0308+0.2551I \quad 0.3\le I<4.0$ $\frac{x}{d}=0.6740+0.0567I \quad 4.0<I\le21.0$ $\frac{x}{d}=1.1875+0.0299I \quad 21.0<I\le445$	$\frac{h_e}{d}=\begin{cases}3.19\left(\frac{x}{d}\right)-0.718\left(\frac{x}{d}\right)^2 & \frac{x}{d}\le1.35\\ 1.32+1.24\left(\frac{x}{d}\right) & 1.35<\frac{x}{d}\le13.5\end{cases}$
Modified NDRC	$\frac{x}{d}=\begin{cases}2\sqrt{G} & G\le1.0 \text{ or } \frac{x}{d}\le2\\ 1+G & G>1.0 \text{ or } \frac{x}{d}>2\end{cases}$ $G=\frac{3.8\times10^{-5}NMV^{1.8}}{f_c^{0.5}d^{2.8}}$	$\frac{h_e}{d}=\begin{cases}3.19\left(\frac{x}{d}\right)-0.718\left(\frac{x}{d}\right)^2 & \frac{x}{d}\le1.35\\ 1.32+1.24\left(\frac{x}{d}\right) & 1.35<\frac{x}{d}\le13.5\end{cases}$
BRL	$\frac{x}{d}=\frac{1.33\times10^{-3}}{d^{2.8}\sqrt{f_c'}}MV^{1.33}$	$\frac{h_e}{d}=1.3\frac{x}{d}$
Chang formula	–	$\frac{h_e}{d}=\left(\frac{61}{V}\right)^{0.25}\left(\frac{MV^2}{d^3f_c'}\right)^{0.5}$
The CEA-EDF formula	–	$\frac{h_e}{d}=\frac{0.3083M^{0.5}V^{0.75}}{d^{1.5}(f_c')^{0.375}}$

the crater phase and $x/d>2$ for the tunnel phase. The spherical cavity expansion model is employed to approximate the tunnel phase of penetration [8,18].

For a rigid projectile, motion and final depth can be calculated when the forces acting on the projectile are known. The passage is modeled by the expansion of a spherical cavity at velocity v_c, surrounded by regions of plastic and incompressible materials. From cavity expansion analysis, the relationship between the radial stress σ_r and the expansion velocity is obtained by:

$$\sigma_r = Sf_c' + \rho v_c^2 \tag{3}$$

where ρ is the density of target material. Based on this relationship the force on the projectile is obtained and finally, using Newton's second law, the penetration depth is calculated, as briefly explained below.

During the crater phase the axial resistant force on the projectile nose is:

$$F_R = cx \qquad x<kd \tag{4}$$

where x is the instantaneous crater depth and c is a constant. In the tunnel region, the axial force is:

$$F_R = \frac{\pi d^2}{4}\left(Sf_c' + N^*\rho v^2\right) \qquad x\ge kd \tag{5}$$

Table 2
Mix proportions of concrete

Material	kg/m^3
Portland cement	393
Water	227
Coarse aggregate (MSA: 6.35 mm)	695
Fine aggregate	918
w/c	0.57

where v is the instantaneous velocity, and S is a dimensionless parameter which is related to the compressive strength of the target. N^* is the projectile nose factor and equal to 0.5 for the spherical case [6,7]. Now by using the continuity of force, velocity, and displacement between two phases (i.e., crater and tunnel) and the boundary condition for each phase (I: $v=V$ at $t=0$; II: $v=0$ at final depth), the depth of penetration x according to [19] is:

$$x = \sqrt{\frac{M}{c}}V \qquad x<kd$$
$$x = \frac{2M}{\pi d^2 N^* \rho} ln\left(1+\frac{N^*\rho V_1^2}{Sf'_c}\right)+kd \quad x\geq kd \tag{6}$$

where M is the projectile mass and V_1 the projectile velocity at the beginning of the tunnel phase:

$$V_1^2 = \frac{MV^2-(\pi kd^3/4)Sf'_c}{M+(\pi kd^3/4)N^*\rho} \tag{7}$$

and,

$$c = \frac{\pi d}{4k}\frac{(N^*\rho V^2+Sf'_c}{(1+(\pi kd^3/4M)N^*\rho)} \tag{8}$$

S is obtained from Eq. (6), as:

$$S = \frac{N^*\rho V^2}{f'_c}\frac{1}{\left(1+\frac{\pi kd^3 N^*\rho}{4M}\right)\exp\left[\frac{\pi d^2(x-kd)N^*\rho}{2M}\right]-1} \tag{9}$$

For each test, S can be calculated based on the recorded impact velocity and the penetration depth according to Eq. (9). It is observed [7] that the concrete compressive strength, f'_c, can define S, which is a dimensionless parameter. Thus, an empirical S–f'_c curve can be generated. This curve could be used to predict penetration depth of other concrete grades according to Eq. (6) [7].

3. Experimental program

Impact tests were performed on square concrete panels of 30.5 cm × 30.5 cm. Specimens having fabric on either one side or both sides were compared with plain concrete panels. Tests were conducted using a gas gun with a barrel of 1.27 cm in diameter and 132 cm in length. The gun used compressed nitrogen gas with a maximum attainable pressure of 10.3 MPa. Pressure in the range of 1–9.6 MPa was used in these tests depending on the desired initial velocities, which were obtained from the calibration curve for each projectile. Except for one case (PC1) in which a spherical bullet was employed, all other tests used the 34 g cylindrical projectiles with 1.27 cm diameter, 2.54 cm length and a sharp head with a 45° angle. The concrete panels were attached to a 1.27-cm-thick steel plate by four C-clamps, one at each corner. The steel plate was at the front side of the panel, and had a circular opening for the projectile to pass through. The same procedure was used to fix all the panels.

To determine the initial velocity, the time it takes for the projectile to pass between two laser beams directed perpendicular to the path of the projectile was measured with a digital timer, and the residual velocity was obtained by analyzing the videos taken by a high speed digital camera. Two cameras were employed: the first one could capture a maximum of 10,000 frames per second and was operated manually. This camera was used for the 3.81-cm-thick specimens. The other camera had a capability of 35,000 frames per second and was used for the 2.54-cm-thick specimens. This camera was computer controlled

Table 3
Test data and calculated results based on NDRC formulas for 3.81-cm-thick samples

Test #	Mass (g)	Initial V. (m/s)	Res. V. (m/s)	Initial E (J)	Final E (J)	ΔE (J)	$\Delta E/t$ (J/cm)	Response	G	x/d	h_s (cm)	h_e (cm)	f'_c (MPa)
PC1	8.3	235	N/A	229.2	N/A	N/A	N/A	UP	0.185	0.86	4.18	2.81	
PC2	34	167	N/A	474.3	N/A	N/A	N/A	P	0.468	1.37	5.06	3.83	41
PC3	34	192	22	623.8	8.2	615.6	161.6	P	0.599	1.55	5.37	4.11	
PP1	34	200	0	677.3	0.0	677.3	177.8	PL	0.656	1.62	5.49	4.23	
PP2	34	189	0	605.6	0.0	605.6	159.0	PL	0.594	1.54	5.35	4.10	40
PP3	34	188	9	602.2	1.4	600.9	157.7	P	0.591	1.54	5.35	4.10	
PZ1	34	187	0	595.4	0.0	595.4	156.3	PB	0.561	1.50	5.28	4.04	
PZ2	34	184	0	576.2	0.0	576.2	151.2	PB	0.545	1.48	5.24	4.00	43
PZ3	34	196	0	655.8	0.0	655.8	172.1	PL	0.612	1.56	5.39	4.14	
PP1[a]	34	187	13	595.4	2.9	592.5	155.5	P	0.679	1.65	5.54	4.27	
PP2[a]	34	186	24	589.6	9.6	580.0	152.2	P	0.673	1.64	5.53	4.26	30
PP3[a]	34	171	9	495.3	1.3	494.0	129.6	P	0.575	1.52	5.31	4.07	

P: perforated (full penetration of the projectile).
PL: perforation limit (projectile was stuck).
UP: unperforated (specimen was punched but projectile bounced).
PB: perforated and then bounced.
x/d: ratio of penetration depth to diameter of projectile.
h_s: scabbing thickness (Eq. (2)).
h_e: perforation thickness (Eq. (2)).
[a] The front face was the loose side.

Table 4
Test data and calculated results based on NDRC formulas for 2.54-cm-thick samples

Test #	Mass (g)	t (cm)	Initial V. (m/s)	Res. V. (m/s)	Initial E (J)	Final E (J)	ΔE (J)	$\Delta E/t$ (J/cm)	Response	G	x/d	h_s (cm)	h_e (cm)	f'_c (MPa)
PC4	34	2.54	99	21	166.1	7.7	158.4	62.4	P	0.189	0.87	4.19	2.83	
PC5	34	2.54	92	11	144.8	1.9	142.9	56.2	P	0.167	0.82	4.10	2.70	30
PC6	34	2.67	82	0	114.4	0.0	114.4	42.9	PB	0.135	0.73	3.96	2.48	
PC7	34	2.54	84	0	121.3	0.0	121.3	47.7	PB	0.132	0.73	3.95	2.46	
PC8	34	2.54	72	0	87.7	0.0	87.7	34.5	PB	0.099	0.63	3.77	2.18	35
PC9	34	2.79	90	0	137.1	0.0	137.1	49.1	PB	0.147	0.77	4.02	2.57	
PP4	34	2.29	142	72	343.0	87.2	255.8	111.9	P	0.413	1.29	4.91	3.70	
PP5	34	2.16	103	34	180.2	19.1	161.1	74.6	P	0.232	0.96	4.35	3.05	30
PP6	34	2.41	89	14	136.1	3.2	132.9	55.1	P	0.180	0.85	4.16	2.78	
PP7	34	2.54	106	0	189.7	0.0	189.7	74.7	PB	0.219	0.93	4.31	2.99	
PP8	34	2.16	95	12	152.8	2.5	150.3	69.6	P	0.180	0.85	4.16	2.78	37
PP9	34	2.54	87	0	129.7	0.0	129.7	51.1	PL	0.155	0.79	4.05	2.63	
PZ4	34	2.29	106	0	191.3	0.0	191.3	83.7	PB	0.220	0.94	4.31	3.00	
PZ5	34	2.29	113	0	215.7	0.0	215.7	94.4	PL	0.245	0.99	4.40	3.12	37
PZ6	34	2.29	123	0	258.1	0.0	258.1	112.9	PB	0.288	1.07	4.55	3.30	
PZ7	34	2.41	131	0	290.2	0.0	290.2	120.2	PL	0.312	1.12	4.62	3.39	
PZ8	34	2.54	143	0	345.5	0.0	345.5	136.0	PL	0.365	1.21	4.78	3.56	39
PZ9[a]	34	2.41	142	17	341.7	4.8	336.9	139.6	P	0.361	1.20	4.77	3.55	

[a] The front face was the loose side.

and was synchronized with the firing mechanism for the gun. To measure the velocity, the camera was calibrated with a length scale before each set of tests to determine the size of the pixels along the projectile flight path. Measuring the residual velocity is not an easy task in the case of concrete samples without fabric, since debris particles also fly off from the back face and make it difficult to identify the projectile.

3.1. Materials

Concrete panels with Type I/II Portland cement, sand and coarse aggregate of 6.35 mm maximum aggregate size were cast. The mix proportion is given in Table 2. The ratios of water, coarse aggregate, and sand to cement by weight were 0.57, 1.76, and 2.33, respectively. Two different fabrics were employed to reinforce the concrete panels: Polypropylene (PP) and Zylon. The Polypropylene fabric was tested by the strip test (ASTM D 5035-95) [20] and yields a maximum load of 450 N and maximum displacement of 50 mm. The tensile strength of the Zylon fabric is 0.8 GPa based on individual yarn strength, and the failure strain is 2.45% [21]. The maximum strength for the Zylon and PP fabric corresponds to 1550 N/cm and 180 N/cm maximum linear load, respectively.

3.2. Specimens

Ten batches with same mix proportions were cast in a mold with three compartments. For each batch, three concrete panels and three control cylinders (10.2 cm × 20.3 cm) were cast. The concrete panels were squares of 30.5 cm × 30.5 cm, with different nominal thickness (2.54 cm or 3.81 cm). For the 2.54-cm-thick samples, the actual thickness ranged from 2.16 cm to 2.80 cm. The thickness has a significant effect on projectile penetration resistance as will be discussed later. A total of 30 samples were prepared, including 9 without fabric. For the samples with fabric, the fabric was placed at the bottom of the mold and concrete was placed on top of the fabric. Another sheet of fabric was then positioned on top of the concrete. No glue was used in the process. The fabric placed on the top did not bond as well with the concrete compared to the fabric at the bottom of the mold.

Different codes were assigned to the specimens: P indicates the panel geometry of the test specimens; C, represent the control specimens without fabric, P the PP fabric and Z the Zylon fabric. For each set numbers 1–3 correspond to the panel thickness of 3.81 cm, and numbers 4–9 represent the 2.54-cm-thick panels. For the 3.81-cm-thick specimens, the testing age was 52 days, while for 2.54 cm samples the testing age was 28 days. Except for samples PP4–PP6 and PZ4–PZ6, which had fabric on one side only, all the other reinforced panels had fabric on both sides. When shooting at the specimens with fabric on both sides the loose side (top side of the mold when casting) was on the back face, except for PP[a] and PZ9[a] samples where the loose side was in the front when testing the panels. For samples with fabric on one side only (PP4–PP6, PZ4–PZ6) the back face contained the tightly bonded fabric.

4. Results and discussion

4.1. Impact response of concrete panels

The results of the impact tests including the initial and residual velocities are presented in Tables 3 and 4. The perforation and scabbing thickness are calculated based on the

Fig. 2. Front and back face damage in a 3.81-cm-thick plain concrete panel (PC2). The projectile perforated the panel.

NDRC method for plain concrete (Eqs. (1) and (2)). The responses of different specimens and their average compressive strength (35 MPa and 38.5 MPa for 2.54- and 3.81-cm-thick specimens, respectively) are also included in the tables. Four response types have been classified, in accordance to the convention used in [3] (i.e., perforated (P) (the projectile passed through the specimen entirely), perforation limit (PL) (projectile was stuck), perforated and then bounced (PB) (the projectile went through the panel and then bounced back), and non-perforated (UP) (panel was punched but the projectile bounced back).

Figs. 2–5 depict the damage induced on the front and back face of plain and fabric protected concrete panels of 3.81 cm nominal thickness. Fig. 2 shows a plain concrete sample where craters formed on the front and back faces of the specimen due to spalling (front face) and scabbing (back face). Brittle failure was observed for all plain concrete specimens, with macroscopic cracks extending through the specimen to the back face, splitting the specimen into four pieces. Whereas all 3.81 cm control specimens (Table 3) reveal perforation with a projectile of 34 g, only one out of three concrete panels protected by PP fabric revealed perforation with loosely bonded PP fabric on the back face and the tightly bonded PP on the front face. This specimen is shown in Fig. 3. Contrary to the control specimens, no macrocracks were observed and the debris from scabbing was contained by the PP fabric. In the other two panels protected by PP fabric, the projectile was not able to perforate the PP fabric. Two types of responses were also observed for the concrete panels protected with loosely bonded Zylon fabric on the back face: either the projectile went through the panel and then bounced back (PB) or the projectile was stuck in the fabric

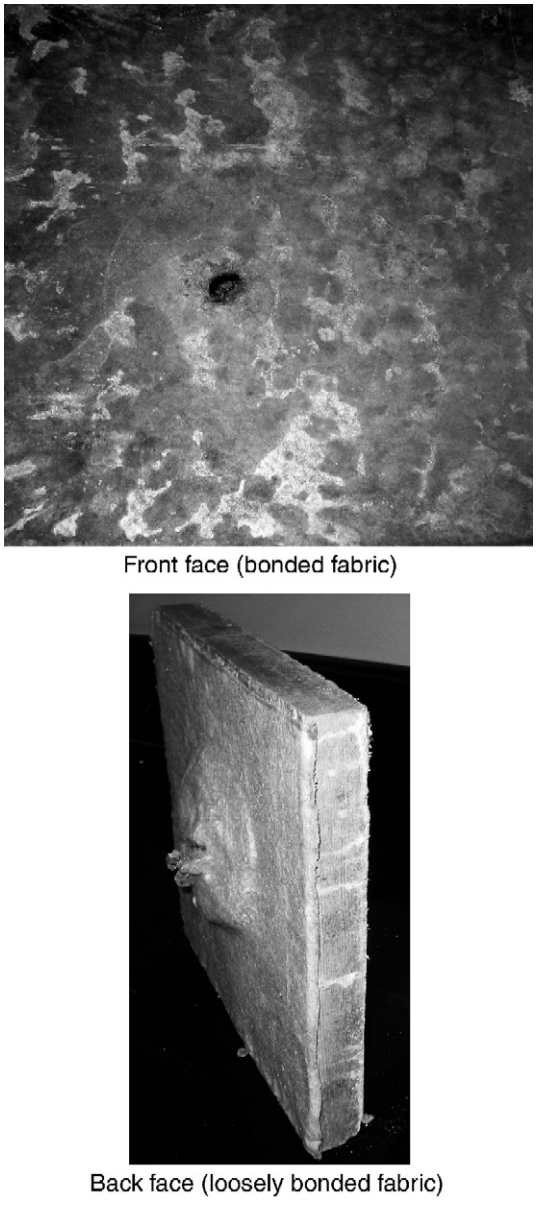

Fig. 3. Front and back face damage in a 3.81-cm-thick concrete panel protected by PP fabric (PP3) on both sides. The projectile perforated the panel but debris due to scabbing from the back face was contained by the PP fabric.

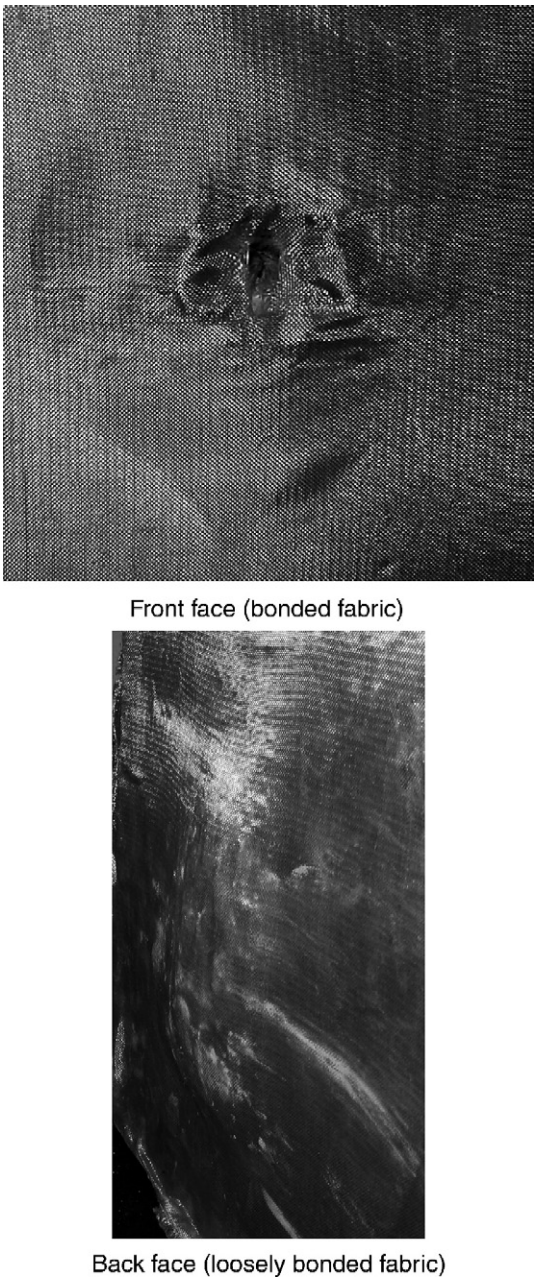

Fig. 4. Damage of front and back face in a 3.81-cm-thick sample protected by Zylon fabric (PZ3).

(PL). The PL response causes a bulge to form on the back face when the concrete panels are protected by either the PP or Zylon fabric as shown in Fig. 4 for a concrete panel protected by Zylon. Both fabrics are able to hold the debris caused by scabbing.

Some impact tests were also performed on specimens with tightly bonded PP fabrics on the back face and loosely bonded PP fabric on the front face to investigate the influence of bonding on impact response. In this case the projectile was able to perforate all three specimens (Table 3). A representative photograph is shown in Fig. 5. Perforation occurred despite a lower initial velocity of 171 m/s compared to PP1–PP3 specimens with loosely bonded fabric on their back faces. Having the loosely bonded fabric on the back face seems to be more effective in catching the projectile.

Figs. 6 and 7 represent the typical damage induced by the projectile in 2.54-cm-thick concrete panels. The initial velocity of the projectile in the 2.54-cm-thick panels was lower compared to the 3.81-cm-thick specimens with and without fabric. Among the 2.54-cm-thick samples, the difference between scabbing and perforation was small (i.e. perforation occurred as soon as scabbing occurred). In the control specimens, the projectile either perforated the panels or it perforated and bounced back (PB). The PB response resulted in multiple macro-crack formations as shown in Fig. 6 but smaller crater sizes compared to Fig. 2. The difference in crater size may be associated with the lower initial velocity of 72 m/s compared to 180 m/s for the 3.81-cm-thick specimen in Fig. 2.

The thinner concrete panels with loosely bonded Zylon fabric on the back face and tightly bonded Zylon fabric on the front face exhibit a PL type of behavior, whereas mainly PB type of behavior was observed for the thicker concrete panels. A difference in response was also observed for the thinner concrete panels protected by PP fabric compared to the thicker panels. Whereas the 3.81-cm-thick specimens with loosely bonded PP fabric on the back face mainly exhibit PL type of behavior, all three types of behavior (P, PB and PL) were observed for the thinner concrete panels protected by PP fabric. Fig. 7 depicts the PL response of a 2.54-cm-thick specimen where a bulge formed and spalling was prevented. Fig. 8 reveals the damage at the back face beneath the PP and Zylon fabric, respectively. In both cases, scabbing occurred beneath the fabrics but the fabrics were able to hold the debris.

The response of the thinner concrete panels to impact loading seems to be less consistent. Furthermore, it is more difficult to correlate the velocities with the corresponding responses. For example, PP7 and PP9 have the same thickness but PP7 exhibits PB whereas PP9 shows PL despite a reduction in velocity

Fig. 5. Damage of back face with bonded fabric in a 3.81-cm-thick sample protected by Polypropylene fabric (PP3[a]).

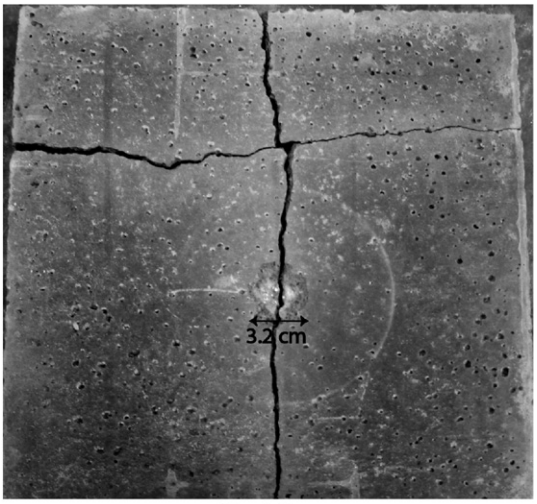

Front face

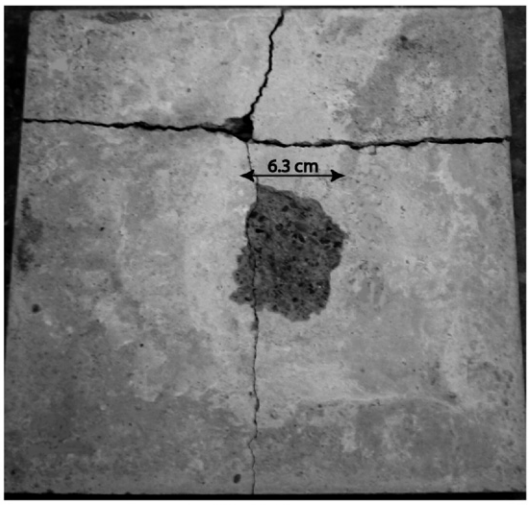

Back face

Fig. 6. Damage of front and back face in a 2.54-cm-thick plain concrete sample (PC8).

of 18%. A more consistent behavior was observed for concrete panels with PP fabric tightly bonded to the back face and no PP fabric at the front surface, despite their differences in initial velocities and specimen thickness. All of these specimens (PP4–PP6) exhibit low penetration resistance and P type response. Consistent P type failure was also observed for the 3.81-cm-thick concrete panels with tightly bonded PP fabric on the back surface and loosely bonded PP fabric at the front face (PP1[a]–PP3[a]). The reduced penetration resistance of panels with PP fabric may be associated with the reduced energy absorbing capacity of the PP fabric if bonded to the back surface. On the other hand, Zylon fabric even if tightly bonded to the back face of concrete panels prevents penetration as shown in Fig. 9. These differences may be explained as follows: The PP fabric is a low strength fabric and the energy is absorbed when the fabric is able to deform, which requires the fabric to be loosely attached to the sample. Zylon fabric on the other hand, requires less deformation for the same energy absorbing capacity due to its high strength. Hence a bonded back face does not impact its energy absorption.

4.2. Energy absorption

Fig. 10 shows the residual velocity as a function of the initial velocity. The residual velocity is zero when perforation is prevented. By increasing the initial velocity for each set it is possible to obtain the velocity in which perforation happens (i.e., residual velocity $\neq 0$). This figure can be used to measure v_{50} (i.e., the velocity in which 50% of panels in each set are perforated). Once perforation of the panels has occurred at a certain critical initial velocity, increasing the initial velocity will increase the residual velocity as shown for PP (2.54) bonded fabric on back face (i.e. PP4–PP6 in Table 4) and PC (2.54) (i.e. PC4–PC9 in Table 4), with an asymptote parallel to the equality line (i.e. $v_{in} = v_{res}$). However, the correlation between initial and residual velocity after perforation could not be established, because the initial velocity would have to be increased beyond 200 m/s for perforation to occur. This was not possible due to

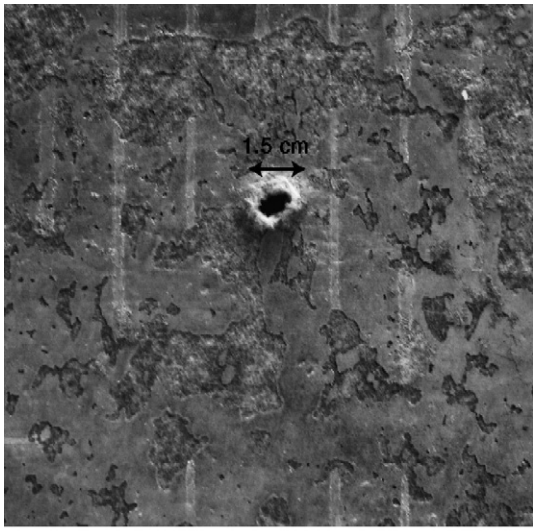

Front face (bonded fabric)

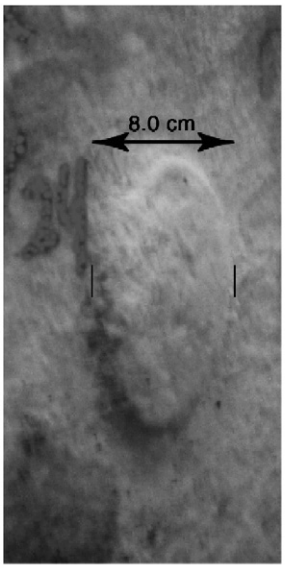

Back face (loosely bonded fabric)

Fig. 7. Damage of front and back face in a 2.54-cm-thick sample protected by Polypropylene fabric (PP9).

the limitation of the maximum allowable pressure of the testing equipment.

Another method to find the perforation velocity is to measure the energy absorbing capacity (ΔE) of the panel in each set. Fig. 11 illustrates the variation in energy absorption as a function of the initial energy for different specimens. As can be observed, almost all the specimens absorbed 100% of the initial kinetic energy. However, the energy absorbing capacity (ΔE) reduces significantly when the thickness decreases from 3.81 cm to 2.54 cm (see Tables 3 and 4). In order to compare the energy absorbing capacity among concrete panels of different thickness, it is more appropriate to measure $\frac{\Delta E}{t}$, where t is the thickness of the target, and ΔE is the change in the kinetic energy of the projectile before and after impact, assuming a constant mass of projectile. Almansa and Canovas [22] reported that $\frac{\Delta E}{t}$ (for perforated samples) is sufficient in characterizing the resistance of concrete due to impact loading associated with a projectile, regardless of velocity or thickness of the target. Furthermore, it was proposed that $\frac{\Delta E}{t}$ is only dependent on the type of concrete (compressive strength, reinforced or unreinforced), and the type of projectile. Hence, it should be constant for each grade of concrete, when using the same projectiles. However, in our tests it is not possible to confirm whether $\frac{\Delta E}{t}$ remains constant due to the limited number of test specimens. But, we can use the results from non-perforated panels (UP, PB, or PL responses) and perforated samples to get a lower bound and upper bound for $\frac{\Delta E}{t}$:

$$\left(\frac{\Delta E}{t}\right)_1 \le \frac{\Delta E}{t} \le \left(\frac{\Delta E}{t}\right)_2$$

$$\left(\frac{\Delta E}{t}\right)_1 = \text{higher value for } \frac{\Delta E}{t} \text{ between shots not having perforated the target} \quad (10)$$

$$\left(\frac{\Delta E}{t}\right)_2 = \text{lower value for } \frac{\Delta E}{t} \text{ between shots having perforated the target}$$

Front face (no fabric)

Back face (bonded fabric)

Fig. 9. Damage of front and back face in a 2.54-cm-thick sample protected by Zylon fabric on one side (back face only) (PZ5).

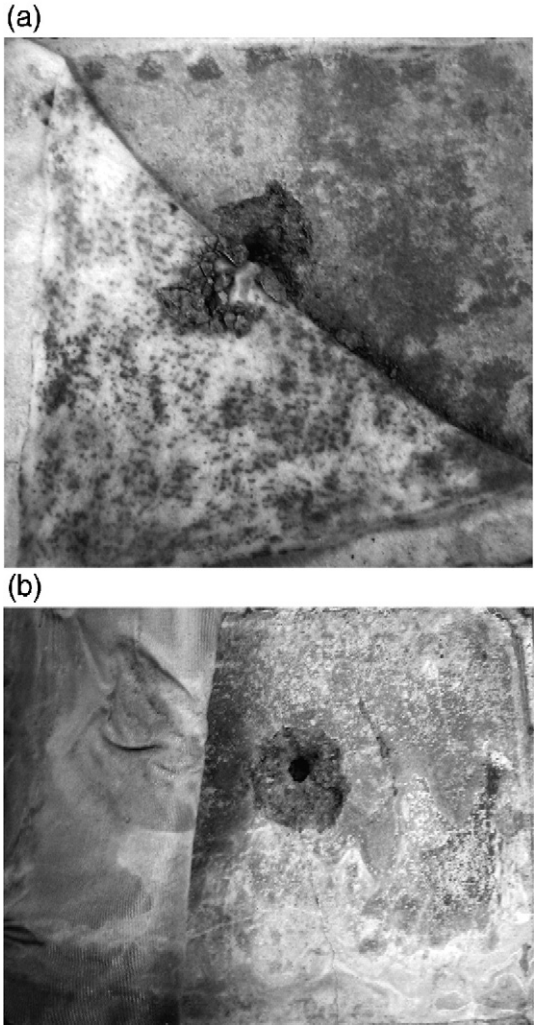

Fig. 8. Typical back face damage beneath the fabric in 2.54-cm-thick samples protected by (a) Polypropylene (PP8) and (b) Zylon fabric (PZ8).

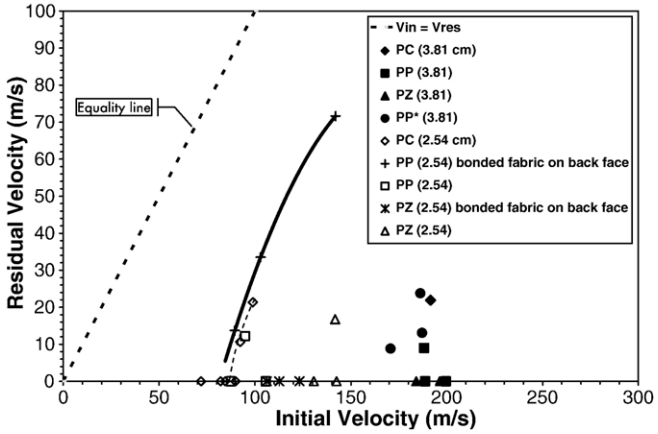

Fig. 10. Residual velocity versus initial velocity.

Based on Eq. (10), the lower bound and upper bound for some sets are measured based on the experimental data from Tables 3 and 4 for concrete panels of different compressive strength:

$$\begin{aligned} &42.9\ (\mathrm{J/cm}) < \left(\frac{\Delta E}{t}\right)_{PC} < 56.2\ (\mathrm{J/cm}) && f'_c = 30\ \mathrm{MPa} \\ &49.1\ (\mathrm{J/cm}) < \left(\frac{\Delta E}{t}\right)_{PC} && f'_c = 35\ \mathrm{MPa} \\ &\left(\frac{\Delta E}{t}\right)_{PC} < 161.6\ (\mathrm{J/cm}) && f'_c = 41\ \mathrm{MPa} \\ &136.0\ (\mathrm{J/cm}) < \left(\frac{\Delta E}{t}\right)_{PZ} && f'_c = 39\ \mathrm{MPa} \\ &172.1\ (\mathrm{J/cm}) < \left(\frac{\Delta E}{t}\right)_{PZ} && f'_c = 43\ \mathrm{MPa} \end{aligned} \quad (11)$$

No bound is obtained for PP samples due to the inconsistency in the test results. These inconsistencies may be associated with the important effect the extent of attachment of the PP fabric to the back face has on the amount of energy that can be absorbed. By comparing the energies for different samples it is seen that adding the Zylon fabric to plain concrete increases $\frac{\Delta E}{t}$ (Table 4).

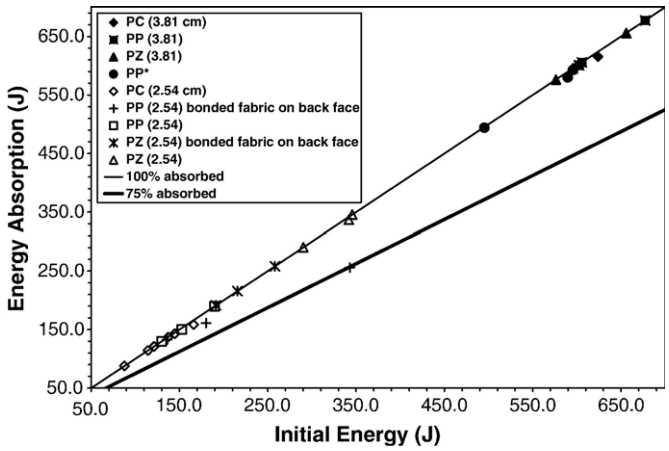

Fig. 11. Energy absorption versus initial energy.

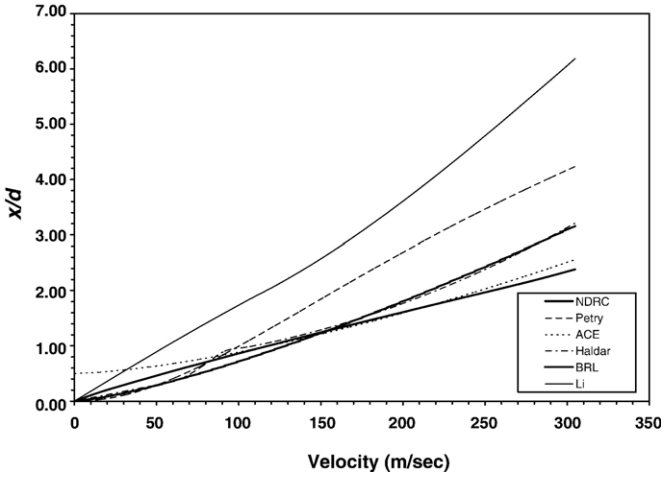

Fig. 12. Variation of penetration depth with impact velocity for different empirical formulas.

For Zylon fabric $\frac{\Delta E}{t}$ is not very sensitive to the thickness, contrary to the plain concrete and PP specimens where an increase in thickness changes $\frac{\Delta E}{t}$ values significantly (see Tables 3 and 4). It is important to note that in the velocity range used for thicker samples (3.81 cm) the concrete itself was able to absorb almost all the kinetic energy and the only effect of the fabric in protected samples was to catch the debris. However, for thinner samples the fabric absorbed some of the impact energy as well.

4.3. Penetration depth

Tables 3 and 4 show the calculated penetration depth ($\frac{x}{d}$), scabbing thickness (h_s) and perforation thickness (h_e) for our tests based on the NDRC approach. Penetration depth is calculated from Eq. (1), and its value used to determine the scabbing and perforation thickness (Eq. (2)). It should be noted that the perforation and scabbing formulas are valid for any thickness, but the penetration depth formulas were derived for thick panels. However, they are commonly used for thickness comparable to our test specimens [14], and are utilized in this study

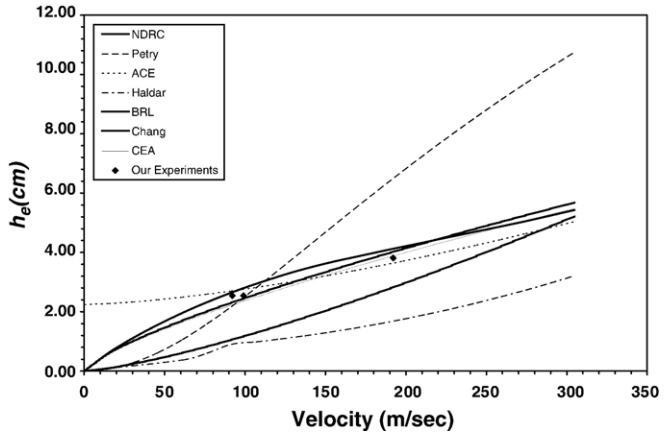

Fig. 13. Variation of perforation thickness vs. impact velocity for different empirical formulas.

to predict penetration. For our thickness, scabbing is inevitable as indicated in Tables 3 and 4 {if $t<h_s \Rightarrow$scabbing}. For the panels protected by fabric, scabbing develops in the concrete, but the fabric is capable of holding the debris. The models are also able to predict the values of the perforation thickness for plain concrete panels {if $t>h_e \Rightarrow$(PL or PB) e.g., PC7–PC9}. For samples protected by fabric, even though the concrete is perforated, the perforation cannot be predicted because the fabric catches the debris and the projectile.

Figs. 12 and 13 present the theoretical results for penetration depth and perforation thickness, using methods in Table 1 for plain concrete panels of 34 MPa compressive strengths, and a projectile of 34 g. By using our velocities, we can check if these models provide reasonable predictions of our experimental results. Based on post-test observations the crater regime is observed when $x/d<2$ [23]. According to Fig. 12 using our experimental velocities for 2.54-cm-thick plain concrete panels (ranging from 72 m/s to 100 m/s) this is indeed the case. The NDRC method provides the average $\frac{x}{d}$ value when compared to all other methods for velocities below 120 m/s. As an example, in PC7–PC9 the average velocity is 82 m/s. Hence using this velocity the predicted x/d is approximately 0.7 (Fig. 12) and the predicted penetration depth x is 0.89 cm for the projectile diameter (1.27 cm) used in our tests, and this result agrees with our experimental results (i.e., no penetration observed for PC7–PC9).

Also, for perforation thickness, Fig. 13 yields a value less than 2.54 cm for the same samples mentioned above, which predicts that our samples will not perforate, as observed experimentally. Also, the results from three perforated panels (PC3–PC5) are depicted in Fig. 13. As observed, these points are close to the NDRC predictions. However, these figures are only practical for plain concrete, since Zylon fabric and PP fabric loosely bonded to the back face of concrete panels successfully prevent perforation.

5. Conclusion

In this paper, experiments were performed to analyze the impact response of concrete panels of different thickness protected by either PP or Zylon fabric. It was found that the thickness of concrete panels has a significant effect on penetration resistance. All targets were able to absorb most of the kinetic energy of the projectiles in our tests. Moreover, in the case of samples protected by fabric, they can effectively catch the debris and hold the scabbed crater from the back face of the targets. Furthermore, PP fabric loosely bonded to the back face was more effective in absorbing the impact energy. Panels protected by Zylon fabric, either on one side or both sided, exhibit a higher energy absorbing capacity compared to plain concrete panels. An upper and lower bound were proposed for $\frac{\Delta E}{t}$ values for plain concrete samples and concrete panels with Zylon. However, these bounds were not attainable for the concrete protected by the PP fabric. For this type of fabric, the extent of bond to the concrete sample plays an important role in the amount of energy absorbed, so it was not possible to set a bound for $\frac{\Delta E}{t}$. NDRC method predictions match our results for plain concrete samples. However, the current penetration formulas are not able to predict the impact parameters for concrete panels protected by fabric.

References

[1] M.E. Backman, W. Goldsmith, The mechanics of penetration of projectiles into targets, Int. J. Eng. Sci. 16 (1978) 1–99.
[2] R.P. Kennedy, A review of procedures for the analysis and design of concrete structures to resist missile impact effects, Nucl. Eng. Des. 37 (1976) 183–203.
[3] D.Z. Yankelevsky, Local response of concrete slabs to low velocity missile impact, Int. J. Impact Eng. 19 (1997) 331–343.
[4] W. Goldsmith, Non-ideal projectile impact on targets, Int. J. Impact Eng. 22 (1999) 95–395.
[5] M.H. Zhang, V.P.W. Shim, G. Lu, C.W. Chew, Resistance of high-strength concrete to projectile impact, Int. J. Impact Eng. 31 (2005) 825–841.
[6] Q.M. Li, D.J. Tong, Perforation thickness and ballistic limit of concrete target subjected to rigid projectile impact, J. Eng. Mech., ASCE 129 (2003) 1083–1091.
[7] Q.M. Li, X.W. Chen, Dimensionless formulae for penetration depth of concrete target impacted by a non-deformable projectile, Int. J. Impact Eng. 28 (2003) 93–116.
[8] M.S. Williams, Modeling of local impact effects on plain and reinforced concrete, ACI Struct. J. 91 (1994) 178–187.
[9] M.J. Forrestal, F.R. Norw, D.B. Lonocope, Penetration into targets described by locked hydrostats and shear strength, Int. J. Solids Struct. 17 (1981) 915–924.
[10] V.K. Luk, M.J. Forrestal, Penetration into semi-infinite reinforced concrete targets with spherical and ogival nose projectiles, Int. J. Impact Eng. 6 (1987) 291–301.
[11] M.J. Forrestal, D.Y. Tzou, A spherical cavity-expansion penetration model for concrete targets, Int. J. Solids Struct. 34 (1997) 4127–4146.
[12] Y. Me-Bar, A method for scaling ballistic penetration phenomena, Int. J. Impact Eng. 19 (1997) 821–829.
[13] A. Schenker, I. Anteby, E. Nizri, B. Ostraich, Y. Kivity, O. Sadot, O. Haham, R. Michaelis, E. Gal, G. Ben-Dor, Foam-protected reinforce concrete structure under impact: experimental and numerical studies, ASCE J. Struct. Eng. 131 (2005) 1233–1242.
[14] A.N. Dancygier, D.Z. Yankelevsky, High strength concrete response to hard projectile impact, Int. J. Impact Eng. 18 (1996) 583–599.
[15] A.N. Dancygier, Rear face damage of normal and high-strength concrete elements caused by hard projectile impact, ACI Struct. J. 95 (1998) 291–304.
[16] X. Lou, W. Sun, S.Y.N. Chan, Characteristics of high-performance steel fiber-reinforced concrete subject to high velocity impact, Cem. Concr. Res. (2000) 907–914.
[17] G.E. Slitter, Assessment of empirical concrete impact formulas, J. Struct. Div., ASCE 106 (1980) 1023–1045.
[18] S.J. Hanchak, M.J. Forrestal, E.R. Young, J.Q. Ehrgott, Perforation of concrete slabs with 48 MPa (7 ksi) and 140 MPa (20 ksi) unconfined compressive strengths, Int. J. Impact Eng. 12 (1992) 1–7.
[19] X.W. Chen, Q.M. Li, Deep penetration of a non-deformable projectile with different geometrical characteristics, Int. J. Impact Eng. 27 (2002) 619–637.
[20] Standard test method for breaking force and elongation of textile fabrics (strip method), Book of ASTM Standards, vol. 07.02, Philadelphia, 2005, pp. 276–283.
[21] D.A. Shockey, J.W. Simons, D.C. Erlich, Improved barriers to engine fragments: interim report I, DOT/FAA/AR-99/8-I, Federal Aviation Administration, Washington DC, 1999.
[22] E.M. Almansa, M.F. Canovas, Behavior of normal and steel fiber-reinforced concrete under impact of small projectiles, Cem. Concr. Res. (1999) 1807–1814.
[23] M.J. Forrestal, B.S. Altman, J.D. Cargile, S.J. Hanckak, An empirical equation for penetration depth of ogive-nose projectiles into concrete targets, Int. J. Impact Eng. 15 (1994) 395–405.